

## Relationships between the surface electronic and chemical properties of doped 4d and 5d late transition metal dioxides

Zhongnan Xu<sup>1</sup> and John R. Kitchin<sup>1, a)</sup>

*Department of Chemical Engineering, Carnegie Mellon University, 5000 Forbes Ave, Pittsburgh, PA 15213*

(Dated: 4 February 2016)

Density functional theory calculations were performed to elucidate the underlying physics describing the adsorption energies on doped late transition metal dioxide rutiles. Adsorption energies of atomic oxygen on doped rutiles  $M^D$ - $M^H$ O<sub>2</sub>, where transition metal  $M^D$  is doped into  $M^H$ O<sub>2</sub>, were expressed in terms of a contribution from adsorption on the pure oxide of the dopant  $M^D$  and perturbations to this adsorption energy caused by changing its neighboring metal cations and lattice parameters to that of the host oxide  $M^H$ O<sub>2</sub>, which we call the ligand and strain effects, respectively. Our analysis of atom projected density of states revealed that the  $t_{2g}$ -band center had the strongest correlation with adsorption energies. We show that charge transfer mediated shifts to the  $t_{2g}$ -band center describe the ligand effect, and the radii of the atomic orbitals of metal cations can predict the magnitude and direction of this charge transfer. Strain produces systematic shifts to all features of the atom projected density of states, but correlations between the strain effect and the electronic structure were dependent on the chemical identity of the metal cation. The slope of these correlations can be related to the idealized  $d$ -band filling. This work elucidates the underlying physics describing adsorption on doped late transition metal oxides and establishes a foundation for models that use known chemical properties for the prediction of reactivity.

---

<sup>a)</sup>Electronic mail: [jkitchin@andrew.cmu.edu](mailto:jkitchin@andrew.cmu.edu)

# I. INTRODUCTION

Accelerated materials discovery is key to the achievement of many of our current technological goals aimed at reducing our dependence on fossil fuels and realizing green production of chemicals.<sup>1,2</sup> Metal oxides catalyze a number of chemical reactions that lie in these focus areas. These applications include hydrogen production via water electrolysis,<sup>3</sup> oxygen reduction for the oxidation of fuels in solid oxide fuel cells (SOFC),<sup>4</sup> conversion of sunlight into chemical energy via photocatalytic water-splitting,<sup>5</sup> and general oxidation/reduction reactions for chemical production.<sup>6-8</sup> The chemical property that dominates trends in the observed activity in many of these applications is the adsorption energy of various intermediate species.<sup>9-12</sup> One strategy to easily tune the adsorption energy to obtain desirable properties is by doping or mixing an oxide with a different transition metal species.<sup>13-15</sup>

Identification of such dopant-host pairs can be accelerated through models that relate their known chemical properties (e.g., electronegativity, atomic size) to desired chemical properties such as adsorption energies. These models already exist for the selection of metal alloy materials in a few applications,<sup>16,17</sup> and their development using density functional theory (DFT) calculations has been illustrated in a number of studies.<sup>18-20</sup> We highlight two strategies used in these studies. One, DFT calculations can be performed in a manner that isolates the interactions that determine the performance of alloys with respect to their pure constituents. From DFT studies, the ligand and strain effect have been identified in metals.<sup>21-23</sup> Two, the electronic structure can be used to relate these effects to both known chemical properties and adsorption energies. For late transition metal surfaces, the adsorption energy can be correlated with the surface projected  $d$ -band center and width, which is then correlated to the atom's interatomic matrix element.<sup>24</sup> In this work, we extend these ideas to adsorption on oxide surfaces.

In this study, we use these two strategies to search for relationships between electronic and chemical properties that describe trends on doped late transition metal oxides. We first decompose the change in the adsorption energy on a specific transition metal oxide when doped into another oxide, which we call a "dopant" effect, into a ligand and strain effect and validate that these two effects can describe the dopant effect. From studying a number of electronic structure features, we find that the center, filling, and width of the  $t_{2g}$ -band of the metal at the adsorption site best describes the trends in adsorption energy.

We then use relationships with features of the  $t_{2g}$ -band to determine that charge transfer between adjacent metal atoms is the primary mechanism of the ligand effect, and the strain effect results in a correlation between the adsorption energy, strain, and properties of the  $t_{2g}$ -band that are dependent on the occupancy of the  $d$ -states. We make simple correlations between known chemical properties and the magnitude of the strain and ligand effect as the groundwork for future predictive models.

## II. METHODS

All calculations were performed using the Vienna Ab-initio Simulation Package (VASP)<sup>25,26</sup> with the Perdew-Burke-Ernzerhof (PBE)<sup>27,28</sup> generalized gradient approximation (GGA) exchange-correlation functional. The core electrons were described by the projector-augmented wave (PAW) method.<sup>29,30</sup> The Kohn-Sham orbitals were expanded with plane-waves up to a 500 eV cutoff. All  $k$ -points were represented on Monkhorst-Pack grids<sup>31</sup> with a  $7 \times 7 \times 1$   $k$ -point grid.

It is well known that the  $d$ -electrons of transition metal oxides contain correlation effects that are not accurately captured using standard GGA exchange correlation functionals, and the inclusion of a Hubbard  $U$  or partial exact exchange is required to capture accurate properties.<sup>32,33</sup> We have not included either of these corrections for a number of reasons. The high computational cost of using hybrid functionals makes it infeasible considering the number of calculations performed in this work. We have neglected the inclusion of the Hubbard  $U$  because we are primarily interested in the adsorption energy trends between different systems and their relationship with the electronic structure. Previous work have shown that neither of these properties change with respect to the Hubbard  $U$ . Work from our group on both oxygen vacancy and adsorption energies on transition metal oxides show that the inclusion of the Hubbard  $U$  does not change trends between different systems.<sup>34,35</sup> In addition, recent work on  $\text{TiO}_2$  doped with transition metals found similar electronic structure correlations with and without the addition of the Hubbard  $U$ .<sup>36</sup>

We calculated the band center, width, and fractional filling of different surface atom projected electronic structure features. The formulas we used are below.

$$E_l = \frac{\int \rho E dE}{\int \rho dE} \quad (1)$$

$$W_l^2 = \frac{\int \rho (E - E_l)^2 dE}{\int \rho dE} \quad (2)$$

$$f_l = \frac{\int_{-\infty}^{E_f} \rho dE}{\int_{-\infty}^{\infty} \rho dE} \quad (3)$$

Given states  $l$ , the band center ( $E_l$ ), was computed as the first moment of the projected density of states about the Fermi level ( $E_f$ ), shown in Equation (1). The band width ( $W_l$ ) is computed as the square-root of the second moment of projected density of states about the band center, shown in Equation (2). The fractional filling ( $f_l$ ) is taken as the integral over states up to the Fermi level divided by the integral over all states, shown in Equation (3).

When studying doped oxides, many theoretical studies examine how a specific material's property is changed by doping in another metal.<sup>37-39</sup> Instead, we approach the problem from a different angle by asking the question, "How are the chemical properties of a specific atom changed when it is doped into another system?" The chemical property we will look at in this study is the dissociative adsorption energy of atomic oxygen. Given dopant atom  $M^D$  and host atom  $M^H$ , we hypothesize that the adsorption energy on  $M^H O_x$  doped with  $M^D$  ( $M^D-M^H O_x$ ), where  $M^D$  is the adsorption site, can be described by the adsorption energy of  $M^D$  in its native oxide  $M^D O_x$  and the perturbations to its electronic structure caused by placing it inside the oxide of the host,  $M^H O_x$ . We break up these perturbations as a strain and ligand effect, which make up what we call a "dopant" effect. This methodology is shown in Figure 1.

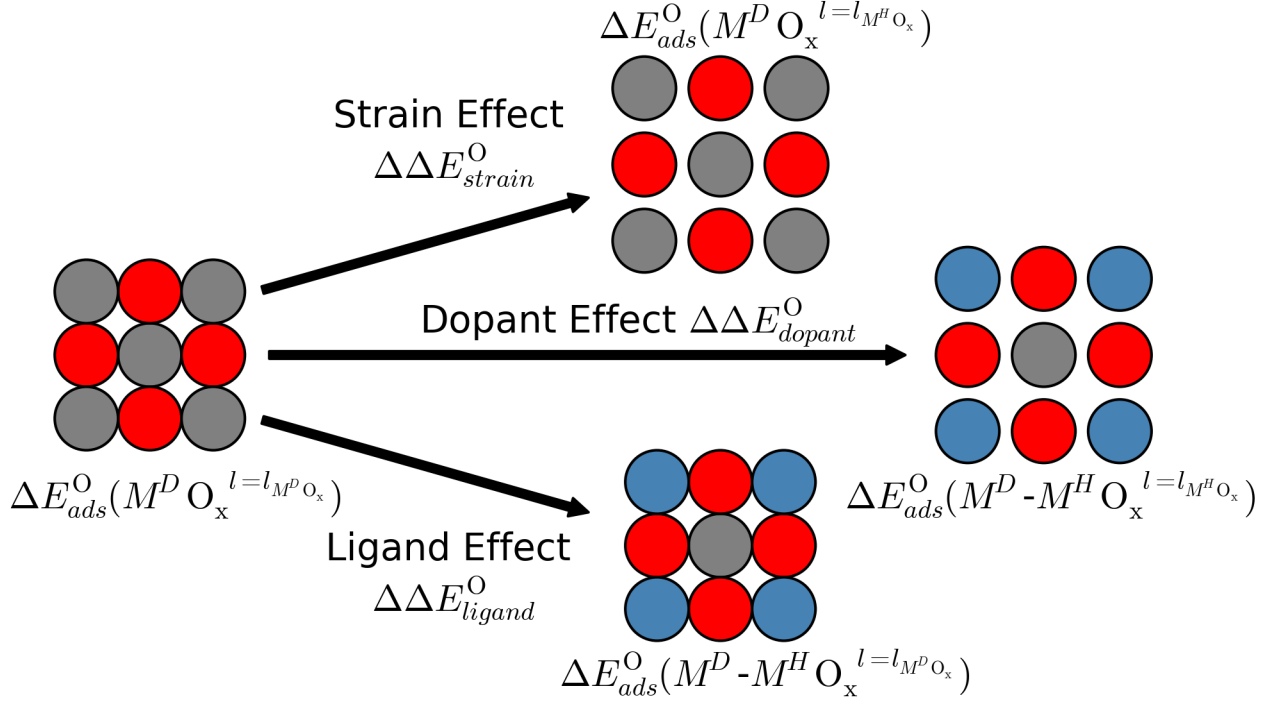


FIG. 1. Illustrates the components, the strain and ligand effect, that produce the change in the adsorption energy upon doping cation  $M^D$  (gray circles) from its native oxide into the oxide of cation  $M^H$  (blue circles), which we call the "dopant" effect. Given a single  $M^D$ - $M^H$  dopant-host pair, adsorption energies on all four systems shown were calculated. With six transition metals studied and not double counting multiple adsorption energies on  $M^D O_2$  in systems with common dopants, this totaled to 96 adsorption energies.

The calculated quantities we require to address this hypothesis are as follows. Given a dopant-host system  $M^D$ - $M^H O_x$  with dopant-host pair  $M^D$ - $M^H$ , we define the ligand, strain, and dopant effects on the adsorption energy of atomic oxygen as differences in adsorption energies shown in the Equations (4), (5), (6) below, respectively.

$$\Delta\Delta E_{ligand}^O = \Delta E_{ads}^O(M^D - M^H O_x^{l=l_{M^D O_x}}) - \Delta E_{ads}^O(M^D O_x^{l=l_{M^D O_x}}) \quad (4)$$

$$\Delta\Delta E_{strain}^O = \Delta E_{ads}^O(M^D O_x^{l=l_{M^H O_x}}) - \Delta E_{ads}^O(M^D O_x^{l=l_{M^D O_x}}) \quad (5)$$

$$\Delta\Delta E_{dopant}^O = \Delta E_{ads}^O(M^D - M^H O_x^{l=l_{M^H O_x}}) - \Delta E_{ads}^O(M^D O_x^{l=l_{M^D O_x}}) \quad (6)$$

$\Delta E_{ads}^O(M^D O_x^{l=l_{M^D O_x}})$ , the reference for the described perturbations, is the adsorption energy

of O onto oxide  $M^D\text{O}_x$  with its lattice parameters,  $l$ , equal to those of its equilibrium structure,  $l_{M^D\text{O}_x}$ .  $\Delta E_{ads}^O(M^D-M^H\text{O}_x^{l=l_{M^D\text{O}_x}})$  is the adsorption energy of O onto the same  $M^D\text{O}_x$  structure with every metal cation except the metal cation at the adsorption site is replaced with  $M^H$ .  $\Delta E_{ads}^O(M^D\text{O}_x^{l=l_{M^H\text{O}_x}})$  is the adsorption energy of O onto a structure of  $M^D\text{O}_x$  except the lattice parameters,  $l$ , are those of the relaxed  $M^H\text{O}_x$  structure ( $l_{M^H\text{O}_x}$ ). Finally,  $\Delta E_{ads}^O(M^D-M^H\text{O}_x^{l=l_{M^H\text{O}_x}})$  is the adsorption energy of O onto an equilibrium  $M^H\text{O}_x$  surface with the adsorption site doped with a  $M^D$  metal atom.

The set of oxides we perform these calculations for is all the possible dopant-host,  $M^D$ - $M^H$ , pairs of six late  $4d$  and  $5d$  transition metals (Ru, Rh, Pd, Os, Ir, Pt) in the +4 oxidation state within the rutile crystal structure. This comes to a total of 30 unique  $M^D$ - $M^H$  pairs. For each dopant-host pair we calculated four separate adsorption energies to evaluate the ligand, strain, and dopant effect. If we do not double count  $M^D$ - $M^H$  pairs that share a common  $M^D$  and therefore the same  $\Delta E_{ads}^O(M^D\text{O}_x^{l=l_{M^D\text{O}_x}})$  calculation, this totals to 96 adsorption energies. All adsorption energies were calculated on the (110) surface in four layer slabs with the top two layers allowed to relax. The adsorption site was the  $5cus$  site with bridge oxygen sites occupied and a  $5cus$  coverage of 0.5 ML, which equates to a  $2 \times 1$  surface unit cell.

Our study focuses on this set of systems for a number of reasons. One, recent work from our group found no universal, surface projected  $d$  or  $p$ -band property which gave strong correlations with adsorption energies for the entire row of  $3d$  transition metal monoxides.<sup>40</sup> Features of the  $d$ -band that interacted with the adsorbate  $p$ -band was determined by whether the cation was an early, mid, or late transition metal. Two, an extensive review on catalysis by doped oxides has identified the category of systems doped with same-valence dopants (SVDs) or flexible-valence dopants (FVDs) that lacked simple rules describing their behavior.<sup>41</sup> In contrast, low-valence dopants (LVDs) and high-valence (HVDs) can be qualitatively understood by simple electron counting rules.<sup>42</sup> We therefore focus our study on dopant-host pairs that constitute SVDs and FVDs, but we believe the principles from our work may also be used for analysis of LVDs and HVDs. Third, all systems we modeled were in the rutile phase, thereby simplifying our interpretation by eliminating changes in the adsorption energy caused by a major changes in the crystal structure.

### III. RESULTS AND DISCUSSION

The organization of our results and discussion is as follows. In Section III A we validate the decomposition of the dopant effect into separate ligand and strain effects. This allows us to investigate relationships between the adsorption energy and the electronic structure within the context of the ligand and strain effects separately in Sections III C and III D, respectively. However, we first look at a number of electronic structure correlations with all adsorption energies in this study to help us pinpoint the key features we should focus our analysis on. This is done in Section III B before analysis of the ligand and strain effect.

#### A. Validation of strain and the ligand effect

As detailed in the methods, we define the ligand, strain, and dopant effect as the change in the adsorption energy of  $M^D$  in the equilibrium structure of  $M^D\text{O}_2$  caused by perturbations of changing its neighboring metal cations (ligand), lattice parameters (strain), and both (dopant), respectively. When studying the dopant effect by directly doping cation  $M^D$  into the lattice of  $M^H\text{O}_2$ , it is likely that both ligand and strain play separate roles in explaining the adsorption energy. It would be convenient if we could study these effects separately and therefore isolate their relationships with chemical and electronic properties.

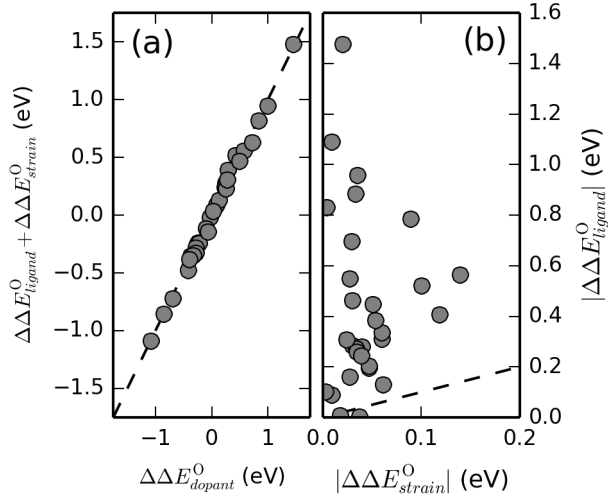


FIG. 2. Validation that the strain and ligand effect can accurately describe the dopant effect (a) and the relative magnitudes of both effects (b) for dopant-host combinations that included all permutations in the set of  $\text{RuO}_2$ ,  $\text{RhO}_2$ ,  $\text{PdO}_2$ ,  $\text{OsO}_2$ ,  $\text{IrO}_2$ , and  $\text{PtO}_2$ .

Figure 2 (a) shows that the simple addition of the ligand and strain effect results in excellent agreement with the dopant effect for all 30 dopant-host pairs considered in this study. This suggests that isolated analysis of both the ligand and strain effect will produce a more complete understanding of the dopant effect. We also find that the absolute value of the ligand effect is up to an order of magnitude higher than the strain effect, shown in Figure 2 (b). This was a surprising result. Because all metal cations form stable +4 oxidation states and metal cations are not typically adjacent in oxide structures, we did not expect significant interactions via charge transfer, which is present in LVD and HVD systems,<sup>39</sup> nor direct orbital overlap of metal orbitals, which characterizes the ligand effect in metal systems.<sup>22</sup> The next step in our analysis is to understand these effects by looking at correlations with the electronic structure.

## B. Identification of electronic structure descriptors

The electronic structure contains all of the information required to relate the structure and composition of the system to its chemical properties and is readily available from DFT calculations.<sup>43</sup> The difficulty lies in extracting the most important features of the electronic

structure. The  $d$ -band model, which relates easily calculated properties such as its center and width to chemical properties, has had large success in metal systems in large part to the simplicity of both their atomic and electronic structure. For example in metal systems, the five  $d$ -orbitals are degenerate in energy and form a single band, though recent work studying Pt overlayers found that the center of the sum of  $d_{xz}$ ,  $d_{yz}$ , and  $d_{z^2}$  states gave better correlations with adsorption than the entire  $d$ -band.<sup>44</sup>

In oxides, the crystal field theory model describes how the degeneracy of the  $d$ -states is lifted into the  $t_{2g}$  and  $e_g$ -states when the transition metal is octahedrally coordinated with six other oxygen molecules.<sup>45</sup> The  $e_g$  ligands point toward the six oxygen cations and therefore form low and high energy bonding and anti-bonding states, while the  $t_{2g}$ -states are non-bonding and energetically lie between the low and high energy  $e_g$ -states. In addition the metal cation's  $d$ -states, the oxygen  $p$ -states also participate in bonding in oxides through interactions with the  $d$ -states of metals. Figure 3 illustrates these characteristics with a sample atom projected density of states (DOS) of the metal cation at the adsorption site and the four surface and one subsurface oxygen atoms bonded to this adsorption site.

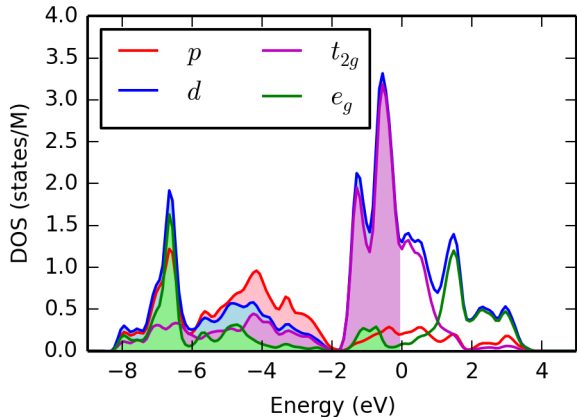


FIG. 3. Sample atom-projected, phase-separated density states of  $\text{RuO}_2$ . Includes the  $d$  (blue),  $e_g$  (purple), and  $t_{2g}$ -states (green) of the cation at the  $5cus$  adsorption site and  $p$ -states (red) of the four surrounding surface and one subsurface coordinated oxygen anion. Shaded regions show occupied states. All densities are normalized on a per atom basis.

Our goal is to correlate features of these states to adsorption energies for the systems we tested. Previous work has already shown correlations of chemical properties of transition

metal oxides with the center of the  $d$ -states,<sup>36,46</sup> center of bulk oxygen  $p$ -states,<sup>47</sup> occupancy of the  $e_g$ -states,<sup>48,49</sup> and occupancy of the  $t_{2g}$ -states.<sup>49</sup> Figure 4 shows correlations between the O adsorption energy of all adsorption energies and the center of the atom projected  $d$ ,  $e_g$ , and  $t_{2g}$ -band of adsorption site and  $p$ -band of the surface oxygen atoms. We found that many correlations exist between the electronic structure features and adsorption for systems with the same element at the adsorption site. The feature that showed the best universal correlations with all adsorption energies was the  $t_{2g}$ -band center. We note that the correlation is dependent on whether the adsorption site is a row 4 or row 5 transition metal. Inspection of the density states reveal that for all of our materials, the  $t_{2g}$  states lie near the Fermi level. This observation is consistent with strong correlations between surface states near the Fermi level and the adsorption energy found for transition metal carbides and doped TiO<sub>2</sub>.<sup>36,50</sup> Now that we have identified that features of the  $t_{2g}$ -states could be a strong descriptor of adsorption, we use this information in our understanding of the underlying physics of the ligand and strain effect.

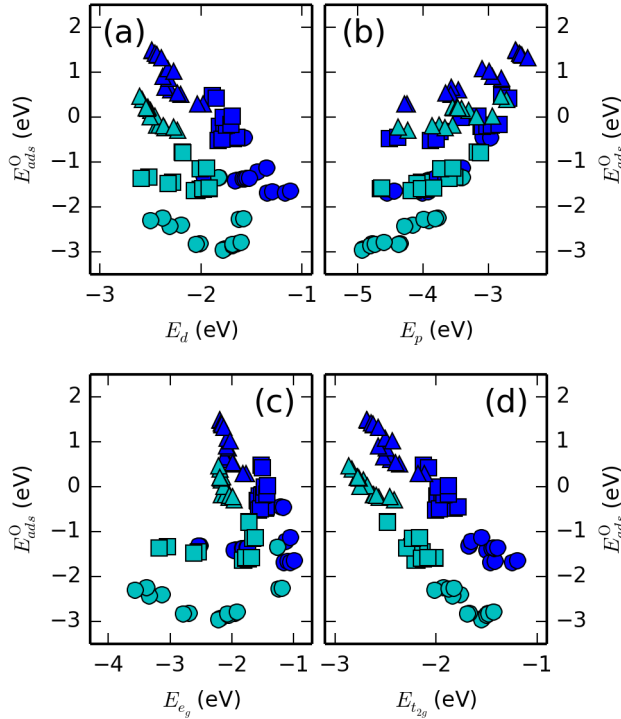


FIG. 4. Correlations of the center of the (a) metal  $d$ -band, (b) oxygen  $p$ -band, (c) metal  $e_g$ -band, and (d) metal  $t_{2g}$ -band with all calculated adsorption energies of atomic oxygen in this study. All properties of the electronic structure were taken from the bare surface. Blue and cyan markers show systems where  $M^D$  is a row 5 and 6 metal, respectively. Circle, square, and triangle markers show systems where  $M^D$  is a column 8, 9, and 10 metal, respectively.

### C. Relationships between the ligand effect and the electronic structure

In the Section III B, analysis of correlations between electronic features and adsorption energies of all systems showed a strong correlation with the center of the  $t_{2g}$ -band. Our goal now is to use this information to uncover the underlying physics of the ligand effect. Figure 5 shows that the ligand effect ( $\Delta\Delta E_{ligand}^O$ ) shows a strong correlation with changes in the center of the  $t_{2g}$ -band ( $\Delta E_{t_{2g}}$ ). Perturbing the dopant  $M^D$  by replacing its  $M^D O_2$  atomic environment with  $M^H$  cations results in shifts to the  $t_{2g}$ -band center and a inverse relationship to its adsorption energy. This relationship is reminiscent of the  $d$ -band model in metals and also observed in previous studies with correlations of the entire  $d$ -band,<sup>36,46</sup> though we found in this case that  $t_{2g}$ -band gave a stronger correlation than the  $d$ -band, the

analysis of which can be found in the supporting information.<sup>51</sup> One explanation for this correlation is that the energies of  $t_{2g}$ -states determines the energies and fillings of the bonding and anti-bonding states of the adsorbed O atom. If the  $t_{2g}$ -states have a lower (higher) center, then the adsorbate anti-bonding states will be less (more) occupied, resulting in stronger (weaker) adsorption.<sup>49</sup>

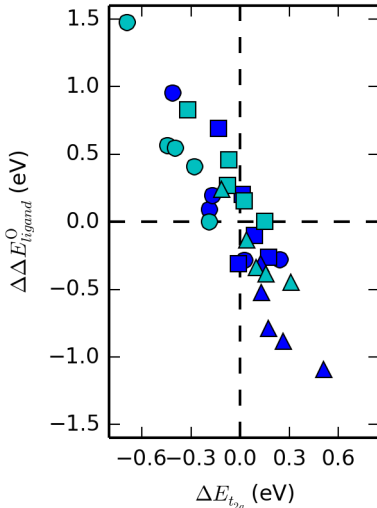


FIG. 5. Relationship between the ligand effect ( $\Delta\Delta E_{ligand}^O$ ) in system  $M^D-M^H O_2$  and the corresponding difference in the center of the  $t_{2g}$ -band ( $E_{t_{2g}}$ ) between the system  $M^D O_2$  and  $M^D-M^H O_2$  with the lattice constant of  $M^D O_2$ . Blue and cyan markers show systems where  $M^D$  is a row 5 and 6 metal, respectively. Circle, square, and triangle markers show systems where  $M^D$  is a column 8, 9, and 10 metal, respectively.

While these observations relate the ligand effect to known relationships between electronic and chemical properties, it is still unclear the exact mechanism of the ligand effect. In metal systems, the ligand effect can be understood by changes in the  $d$ -band center caused by overlap between atomic orbitals of neighboring atoms that resulted in changes to the shape of the  $d$ -band but conservation of total states.<sup>22,52</sup> Figure 6 (a) hints that a similar mechanism might explain ligand effect in oxides by showing linear correlations between the  $t_{2g}$ -band width and center, which is observed for the ligand effect in metals. Also similar to the ligand effect in metals is that metal cations in the same column lie on the same correlation.<sup>24</sup> However, unique to the ligand effect on oxides is that the filling of the  $t_{2g}$ -band

is not constant. Figure 6 (b) demonstrates that the changes in the center of the  $t_{2g}$ -band are caused by changes in the number of occupied states. Interestingly, increases in the number states, which we expected to result in a more noble-like character of the metal cation, results in positive shifts in the  $t_{2g}$ -band center, which describes less noble-like character and hence a stronger adsorption energy (Figure 5). Upon analyzing relationships between the filling of the  $t_{2g}$  and  $e_g$ -band, we concluded that this change did not come from redistribution of states within the  $d$ -band and that it results from charge transfer with neighboring atoms.

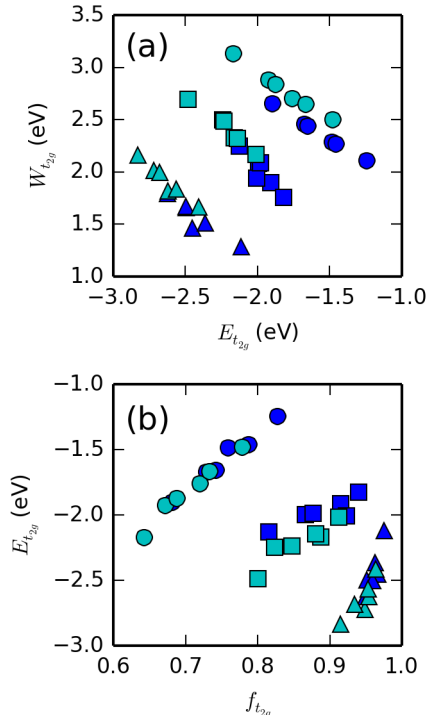


FIG. 6. Relationship between the (a)  $M^D$   $t_{2g}$ -band center ( $E_{t_{2g}}$ ) and width ( $W_{t_{2g}}$ ) and the (b)  $M^D$   $t_{2g}$  fractional filling ( $f_{t_{2g}}$ ) and center ( $E_{t_{2g}}$ ) of systems where  $M^D$  is either in its native lattice  $M^D\text{O}_2$  or is under the ligand effect,  $M^D\text{-}M^H\text{O}_2$   $l=l_{M^D\text{O}_2}$ . Blue and cyan markers show systems where  $M^D$  is a row 5 and 6 metal, respectively. Circle, square, and triangle markers show systems where  $M^D$  is a column 8, 9, and 10 metal, respectively.

To investigate whether the addition or loss of electrons on the metal cation produced by the ligand effect comes from charge transfer with neighboring oxygen cations, we correlate changes of the fractional filling of both the  $d$ -states and oxygen  $p$ -states caused by the ligand effect (Figure 7 (a)). Surprisingly, we find an increase/decrease in the fractional filling of

the  $d$ -states caused by the ligand effect results in a corresponding increase/decrease in the fractional filling of the  $p$ -states of neighboring oxygen cations. This means that oxygen cations only mediate the charge transfer and are not the source of it.

We hypothesize that the source of the charge transfer to  $M^D$  under the ligand effect must come from the host  $M^H$  cations. To test this hypothesis, we relate changes in the fractional filling of the oxygen  $p$ -states ( $\Delta f_p$ ) under the ligand effect, where the dopant-host pair is  $M^D$ - $M^H$ , to changes in the fractional filling of the  $d$ -band of the host metal cation  $M^H$  when it is doped into the  $M^D\text{O}_2$  system ( $\Delta f_d^{host}$ ). If our hypothesis is correct, we should observe an inverse relationship between  $\Delta f_p$  and  $\Delta f_d^{host}$ , implying charge from  $M^H$  was transferred to the oxygen in an  $M^D$  environment. Figure 7 (b) shows that this is case, where the slope of the relationship is close to  $\Delta f_p = -\Delta f_d^{host}$ . This is clear evidence that changes in the charge on the  $M^D$  caused by the ligand effect come from electrons transferred from  $M^H$  cations. We note that charge transfer is still evident even when the formal oxidation state of all these species is expected to be +4.

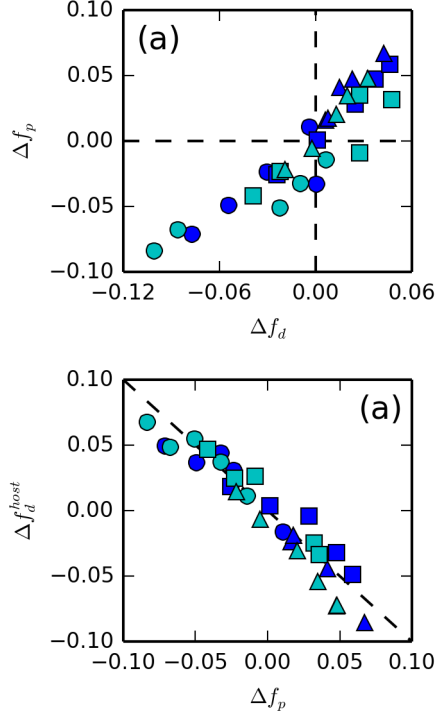


FIG. 7. (a) Relationship between the change on the  $M^D$   $d$ -band filling ( $\Delta f_d$ ) and bonded oxygen  $p$ -band filling ( $\Delta f_p$ ) caused by the ligand effect. Black dashed lines show the  $x=0$  and  $y=0$  axis. (b) Relationship between the change in the bonded oxygen  $p$ -band filling ( $\Delta f_p$ ) caused by the ligand effect in system  $M^D$ - $M^H$ O<sub>2</sub> and the change in the  $M^H$   $d$ -band filling ( $\Delta f_d^{host}$ ) caused by the ligand effect in system  $M^H$ - $M^D$ O<sub>2</sub>. Black dashed line in (b) shows the  $\Delta f_d^{host} = -\Delta f_p$  line. Blue and cyan markers show systems where  $M^D$  is a row 5 and 6 metal, respectively. Circle, square, and triangle markers show systems where  $M^D$  is a column 8, 9, and 10 metal, respectively.

Having understood the nature of the ligand effect, we now wish to understand what properties of the dopant-host pair determines the direction and magnitude of the charge transfer. We first suspected differences in their electronegativities should correlate with the ligand effect, but we did not find this to be the case. We went back to calculated electronic properties, and we found that the difference between the widths of their  $t_{2g}$ -states correlates the best with the ligand effect (Figure 8 (a)). Recent work from our group found that the  $d$ -band width of metal cations in perovskites has a linear correlation with the effective orbital radius raised to the 3/2 power ( $r_d^{3/2}$ ).<sup>53</sup> Our results therefore suggests that differences in  $r_d^{3/2}$  of the dopant-host pair should also correlate with the ligand effect. Figure 8 (b) shows that

this is the case. Though the correlation of the ligand effect with the differences in effective orbital radius is weaker than the correlation with the difference in the calculated  $t_{2g}$ -band width, we emphasize that  $r_d^{3/2}$  is a known chemical property that can be looked up from solid state tables.<sup>54</sup> We believe this observation can be the foundation of future work that creates predictive models of adsorption energies on oxides.

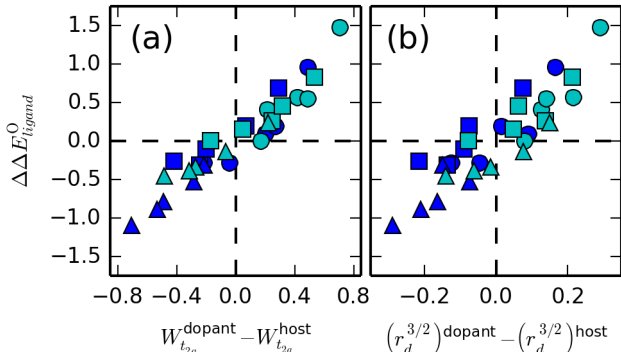


FIG. 8. Relationship between the ligand effect ( $\Delta\Delta E_{ligand}^O$ ) in the dopant-host system  $M^D$ - $M^H$ O<sub>2</sub> and the difference in (a) the  $t_{2g}$ -band width ( $W_{t_{2g}}$ ) and (b) the tabulated effective orbital radius to the 3/2 power ( $r_d^{3/2}$ ) of dopant  $M^D$  and host  $M^H$ . Black dashed line in both (a) and (b) show the  $x=0$  and  $y=0$  axis. Blue and cyan markers show systems where  $M^D$  is a row 5 and 6 metal, respectively. Circle, square, and triangle markers show systems where  $M^D$  is a column 8, 9, and 10 metal, respectively.

Correlations shown in Figures 5 – 8 have a number of implications of the underlying physics dominating the ligand effect. Figure 8 shows that a dopant cation  $M^D$  with a larger  $t_{2g}$ -band width and  $r_d$  effective orbital radius than its host cation  $M^H$  would experience a more endothermic adsorption with respect to  $M^D$ O<sub>2</sub>. According to Figure 5 and 6, the  $t_{2g}$ -band center would shift down to lower energies, in turn implying that charge was transferred away from the  $M^D$  (Figure 6 (b)).

In short, a  $M^D$  dopant with a larger/smaller atomic radius than it's  $M^H$  host loses/gains electrons from  $M^H$  (see Figure 3 in Supporting Information<sup>51</sup>). We hypothesize the nature of this interaction below. If a  $M^D$  is placed into an environment where its  $r_d$  is larger/smaller than the  $M^H$ 's, there will be an increase/decrease in the overlap between the  $M^D$  orbital and oxygen  $p$  orbital, resulting in the creation of hybridized states. Due to Pauli Repulsion, these states will be less/more energetically stable than hybridized states by replaced  $M^H$  with a

smaller/larger  $r_d$  term. If an increase in overlap creates less stable states, charge transfer towards the  $M^H$  host cations will ensue to lower the energy of these states. Likewise, if a decrease in the overlap results in more stable states, these states will be filled with electrons from the  $M^H$  host cations. This charge transfer creates shifts in the center of the  $t_{2g}$ -band, which in turn leads to changes in the adsorption energy on the  $M^D$  cation (see Figure 4 in the Supporting information<sup>51</sup>).

#### D. Relationships between strain and the electronic structure

Having understood the nature of the ligand effect and established correlations between the adsorption energy and both the chemical and electronic properties, we now move on towards the strain effect, which is an order of magnitude smaller than the ligand effect (Figure 2 (b)). This result is consistent with those found by a previous study from our group, which determined that the effect of strain is much smaller compared to changes in  $d$ -band filling.<sup>46</sup> However, in that study correlations between the adsorption energy and  $d$ -band center of strained  $3d$  perovskites were dominated by the number of  $d$ -electrons, and the subtle relationship between the electronic structure and the adsorption energy in the context of strain remained elusive.

Figure 9 shows that the effect of strain on the change in the adsorption energy is unique to the metal cation undergoing strain. This observation is consistent with those found in previous results on oxides<sup>46</sup> and metals.<sup>55</sup> Interestingly, we see that only adsorption on noble metal cations Pd and Pt becomes more endothermic with the application of compressive strain, while the opposite is true the rest of the metal cations. This behavior is in contrast to metals, where compressive strain generally results in endothermic adsorption energies of all late transition metals.<sup>21</sup>

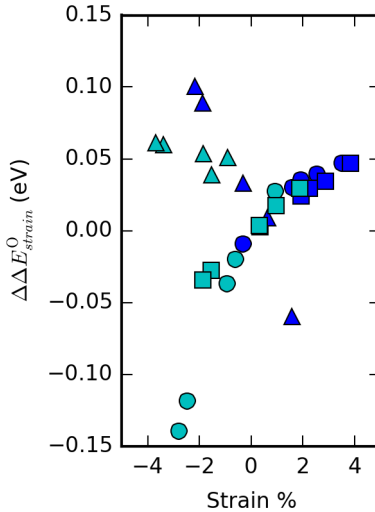


FIG. 9. Relationship between the relative strain in the direction parallel to the surface and the change in the adsorption caused by the strain ( $\Delta\Delta E_{strain}^O$ ). Blue and cyan markers show systems where  $M^D$  is a row 5 and 6 metal, respectively. Circle, square, and triangle markers show systems where  $M^D$  is a column 8, 9, and 10 metal, respectively.

To understand these correlations, we examine relationships between strain and the electronic structure. Because the  $d$ -band width is related to the amount of overlap between the interatomic matrix elements of neighboring atoms, compressive/tensile strain should result in an increase/decrease in the  $d$ -band width. This observation has already been observed for bulk perovskites.<sup>53</sup> Figure 10 (a) shows this to be the case for the  $t_{2g}$ -band as well in rutile dioxides. Furthermore, we also observe a positive correlation between strain the  $t_{2g}$ -band center. The inverse and proportional relationship of strain with changes in the  $t_{2g}$ -band center and width, respectively, also imply that in the context of strain, the  $t_{2g}$ -band center and width have an inverse relationship. In contrast to the ligand effect, which is also mediated by differences in the overlap of atomic orbitals, we found no charge transfer (see supporting information<sup>51</sup>). We attribute this to the symmetry of the strain effect, where the strain induced change in the overlap of atomic orbitals is experienced equally among all metal cations, while the ligand effect produces an asymmetric change that results in charge transfer. This observation suggests in response to strain-induced changes in the  $t_{2g}$ -band width, the  $t_{2g}$ -band center must shift to conserve states, which is consistent with models established on transition metals.<sup>21,55</sup>

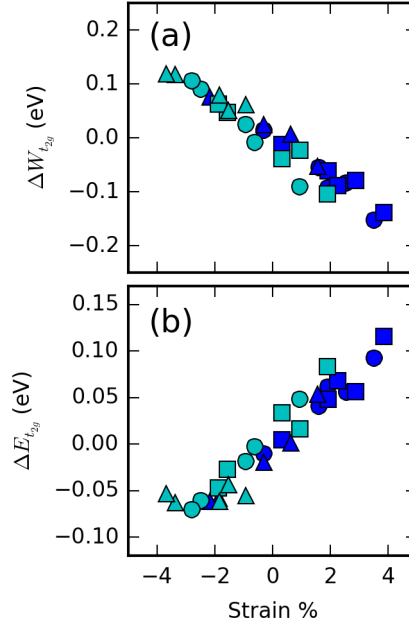


FIG. 10. Relationship between the relative strain in the direction parallel to the surface and the change in the (a)  $t_{2g}$ -band width ( $\Delta W_{t_{2g}}$ ) and (b)  $t_{2g}$ -band center ( $\Delta E_{t_{2g}}$ ). Blue and cyan markers show systems where  $M^D$  is a row 5 and 6 metal, respectively. Circle, square, and triangle markers show systems where  $M^D$  is a column 8, 9, and 10 metal, respectively.

These correlations between strain and the features of the  $t_{2g}$ -states imply one can estimate changes to the electronic structure based on the strain, and these correlations are independent of the metal cation studied. However, Figure 9 and 10 suggests that correlations between the electronic structure and adsorption energy *are not* independent of the metal cation studied. This implication is shown to be true in Figure 11 (a). Note that due to the linear correlations between strain and the  $t_{2g}$ -band center shown in Figure 10 (b), the relationships between the  $t_{2g}$ -band center and the strain effect largely mirror relationships between the amount of strain itself and the strain effect shown in Figure 9. We therefore conclude that the element specific correlation between strain and the adsorption energy is due to each element's unique relationships between the electronic structure and adsorption energy. This is not observed for metal systems, where it is found that despite the relationship between strain the electronic structure, for both early and late transition metals the correlations between the electronic structure and the adsorption energy were the same.<sup>21,55</sup>

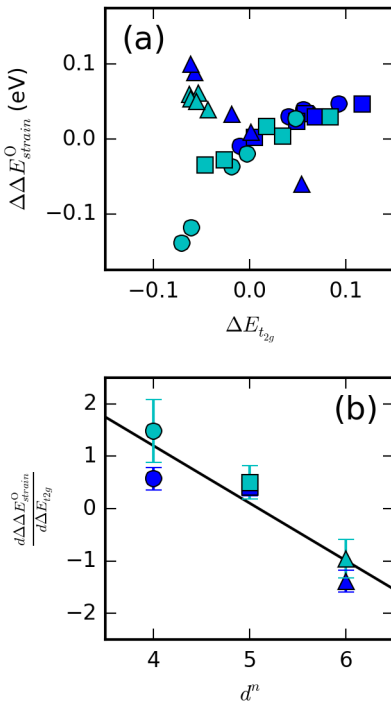


FIG. 11. (a) Relationship between the change in the  $t_{2g}$ -band center ( $\Delta E_{t_{2g}}$ ) due to strain and the change in the adsorption energy due to strain ( $\Delta\Delta E_{strain}^O$ ) (b) Relationship between the idealized occupancy of the  $d$ -states of  $M^D$  and the fitted slope of the relationship between shown in (a) for different  $M^D$  dopants. Errorbars in (b) are the 95% confidence intervals of the fit in (a). Blue and cyan markers show systems where  $M^D$  is a row 5 and 6 metal, respectively. Circle, square, and triangle markers show systems where  $M^D$  is a column 8, 9, and 10 metal, respectively.

Following our ability to predict changes in the electronic structure produced by strain (Figure 10), our final goal is to obtain some insight into the nature for the element specific relationships between the  $t_{2g}$ -band center and the adsorption energy found in Figure (11). We found that the slope of this relationship ( $\frac{d\Delta\Delta E_{strain}^O}{d\Delta E_{t_{2g}}}$ ) was inversely proportional to the idealized filling of the  $d$ -band. Metal cations with an idealized  $d$ -band that was over half filled (Pt and Pd) obey the model that is observed in Figure 4 (d) and 5 for the ligand effect, where a downshift in the  $t_{2g}$ -band produces more endothermic adsorption energies. However, metal cations with the  $d$ -band at half filling or lower show the opposite behavior. We note that this observation necessitates the deconvolution of the dopant effect into the ligand and strain effect, since their effects on reactivity do not follow the same electronic

structure-adsorption relationships. In fact, the larger magnitude of the ligand effect (Figure 2 (b)) probably dominates the observed correlation between the  $t_{2g}$ -band center and the adsorption energy found for all adsorption energies in Figure 4 (d).

The underlying physics that describe the relationship between strain and the adsorption energies eludes us but warrants some discussion. The key difference between the ligand and strain effect is that ligand-induced changes to the electronic structure arise from charge transfer and strain-induced changes to the electronic structure arise from differences in the overlap of atomic orbitals, which altered the widths of many features of the electronic structure (see supporting information<sup>51</sup>). Changes to the shape of both the  $e_g$  and  $t_{2g}$ -band have complex interactions with the adsorption energy. For example, a recent study from our group showed that low energy, bonding orbitals of the  $e_g$ -states are responsible for the stabilization of surface-adsorbate bonds, while high energy, anti-bonding  $e_g$ -states serve to destabilize the bond.<sup>40</sup> While we did find systematic changes to the width of the  $e_g$ -band caused by strain, we could not find simple correlations between the width, center, and filling between the  $e_g$ -band and the strain effect. However, we expect changes in the  $e_g$ -band width and center due to strain causes shifts in energy to both the  $e_g$  bonding and anti-bonding states, which we found difficult to quantify. One possible strategy would be take into account the shape of the  $t_{2g}$  and/or  $e_g$  band. This has been done on transition metals using the band width<sup>56</sup> and the Newns-Anderson model.<sup>57</sup> However, we speculate these interactions are somehow manifest in correlations of the strain effect with the center of the  $t_{2g}$ -band – which is more easily characterized than the  $e_g$  band – and the relationship of  $\frac{d\Delta\Delta E_{strain}^O}{d\Delta E_{t_{2g}}}$  with the idealized  $d^n$  filling shown in Figure 11.

#### IV. CONCLUSIONS

In summary, we have performed DFT calculations to understand the underlying physics that dominate the trends in the dissociative adsorption energy of oxygen on doped transition metal oxides. We express adsorption energies on doped rutiles  $M^D$ - $M^H$ O<sub>2</sub> as a combination of adsorption on the pure oxide of the dopant  $M^D$ O<sub>2</sub> and perturbations to this adsorption energy caused by changing its neighboring metal cations and lattice constant, which we call the ligand and strain effect, respectively.

After validating that the ligand and strain effect can describe the dopant effect, we

developed an understanding of the underlying physics of both the ligand and strain effect on the adsorption energy by relating both of these effects to changes in the electronic structure. We found that the ligand effect is expressed as changes to the  $t_{2g}$ -band center that mirror the  $d$ -band model on metal systems. Changes to the  $t_{2g}$ -band center from the ligand effect are caused by charge transfer between the dopant and host metal cation, mediated by the lattice oxygen. We were able to correlate the magnitude and direction of the ligand effect to differences in the radii of dopant and host metal cation and discussed the physical nature of this mechanism.

Strain systematically changes the widths of many features of the electronic density of states, but in contrast to the ligand effect, strain induced changes to the adsorption energy and  $t_{2g}$ -band center do not follow the same electronic structure correlation that describes the ligand effect or those found in metal systems. In spite of the elusive underlying physical mechanisms that explain the strain effect, we found that the idealized filling of the  $d$ -band can describe the slopes of correlations between changes in the  $t_{2g}$ -band center and the strain effect. This work introduces a number of novel techniques and relationships that elucidate the underlying physics of adsorption on doped oxides and establishes a ground work for possible predictive models reactivity of doped oxides.

## ACKNOWLEDGMENTS

JRK gratefully acknowledges partial support from the DOE Office of Science Early Career Research program (DE-SC0004031).

## REFERENCES

- <sup>1</sup>J. K. Nørskov and T. Bligaard, “The catalyst genome,” [Angew. Chem. Int. Edit.](#) **52**, 776–777 (2013).
- <sup>2</sup>A. Jain, S. P. Ong, G. Hautier, W. Chen, W. D. Richards, S. Dacek, S. Cholia, D. Gunter, D. Skinner, G. Ceder, and K. A. Persson, “Commentary: The materials project: A materials genome approach to accelerating materials innovation,” [APL Mat.](#) **1**, 011002 (2013).
- <sup>3</sup>H. Dau, C. Limberg, T. Reier, M. Risch, S. Roggan, and P. Strasser, “The mechanism

- of water oxidation: From electrolysis via homogeneous to biological catalysis,” *ChemCatChem* **2**, 724–761 (2010).
- <sup>4</sup>Z. Shao and S. M. Haile, “A high-performance cathode for the next generation of solid-oxide fuel cells,” *Nature* **431**, 170–173 (2004).
- <sup>5</sup>A. Fujishima, “Electrochemical photolysis of water at a semiconductor electrode,” *Nature* **238**, 37–38 (1972).
- <sup>6</sup>X. Xie, Y. Li, Z.-Q. Liu, M. Haruta, and W. Shen, “Low-temperature oxidation of CO catalysed by  $\text{Co}_3\text{O}_4$  nanorods,” *Nature* **458**, 746–749 (2009).
- <sup>7</sup>W.-P. Zhou, W. An, D. Su, R. Palomino, P. Liu, M. G. White, and R. R. Adzic, “Electrooxidation of methanol at  $\text{SnO}_x$ -Pt interface: A tunable activity of tin oxide nanoparticles,” *J. Phys. Chem. Lett.* **3**, 3286–3290 (2012).
- <sup>8</sup>J. Graciani, K. Mudiyansele, F. Xu, A. E. Baber, J. Evans, S. D. Senanayake, D. J. Stacchiola, P. Liu, J. Hrbek, J. F. Sanz, *et al.*, “Highly active copper-ceria and copper-ceria-titania catalysts for methanol synthesis from  $\text{CO}_2$ ,” *Science* **345**, 546–550 (2014).
- <sup>9</sup>J. K. Nørskov, J. Rossmeisl, A. Logadottir, L. Lindqvist, J. R. Kitchin, T. Bligaard, and H. Jonsson, “Origin of the overpotential for oxygen reduction at a fuel-cell cathode,” *J. Phys. Chem. B* **108**, 17886–17892 (2004).
- <sup>10</sup>I. C. Man, H.-Y. Su, F. Calle-Vallejo, H. A. Hansen, J. I. Martínez, N. G. Ínoğlu, J. Kitchin, T. F. Jaramillo, J. K. Nørskov, and J. Rossmeisl, “Universality in oxygen evolution electrocatalysis on oxide surfaces,” *ChemCatChem* **3**, 1159–1165 (2011).
- <sup>11</sup>K. S. Exner, J. Anton, T. Jacob, and H. Over, “Controlling selectivity in the chlorine evolution reaction over  $\text{RuO}_2$ -based catalysts,” *Angew. Chem. Int. Edit.* **53**, 11032–11035 (2014).
- <sup>12</sup>G. Chen, Y. Zhao, G. Fu, P. N. Duchesne, L. Gu, Y. Zheng, X. Weng, M. Chen, P. Zhang, C.-W. Pao, *et al.*, “Interfacial effects in iron-nickel hydroxide–platinum nanoparticles enhance catalytic oxidation,” *Science* **344**, 495–499 (2014).
- <sup>13</sup>V. Shapovalov and H. Metiu, “Catalysis by doped oxides: CO oxidation by  $\text{Au}_x\text{Ce}_{1-x}\text{O}_2$ ,” *J. Catal.* **245**, 205–214 (2007).
- <sup>14</sup>P. Liao, J. A. Keith, and E. A. Carter, “Water oxidation on pure and doped hematite (0001) surfaces: Prediction of Co and Ni as effective dopants for electrocatalysis,” *J. Am. Chem. Soc.* **134**, 13296–13309 (2012).
- <sup>15</sup>N. B. Halck, V. Petrykin, P. Krtil, and J. Rossmeisl, “Beyond the volcano limitations in

- electrocatalysis–oxygen evolution reaction,” *Phys. Chem. Chem. Phys.* **16**, 13682–13688 (2014).
- <sup>16</sup>N. İnođlu and J. R. Kitchin, “Identification of sulfur-tolerant bimetallic surfaces using DFT parametrized models and atomistic thermodynamics,” *ACS Catal.* **1**, 399–407 (2011).
- <sup>17</sup>H. Xin, A. Holewinski, and S. Linic, “Predictive structure–reactivity models for rapid screening of Pt-based multimetallic electrocatalysts for the oxygen reduction reaction,” *ACS Catalysis* **2**, 12–16 (2012).
- <sup>18</sup>B. Hammer and J. Nørskov, “Why gold is the noblest of all the metals,” *Nature* **376**, 238–240 (1995).
- <sup>19</sup>B. Hammer, Y. Morikawa, and J. K. Nørskov, “CO chemisorption at metal surfaces and overlayers,” *Phys. Rev. Lett.* **76**, 2141 (1996).
- <sup>20</sup>N. İnođlu and J. R. Kitchin, “New solid-state table: Estimating d-band characteristics for transition metal atoms,” *Mol. Simulat.* **36**, 633–638 (2010).
- <sup>21</sup>M. Mavrikakis, B. Hammer, and J. K. Nørskov, “Effect of strain on the reactivity of metal surfaces,” *Phys. Rev. Lett.* **81**, 2819 (1998).
- <sup>22</sup>J. Kitchin, J. K. Nørskov, M. Barteau, and J. Chen, “Modification of the surface electronic and chemical properties of Pt (111) by subsurface 3d transition metals,” *J. Chem. Phys.* **120**, 10240–10246 (2004).
- <sup>23</sup>T. A. Maark and A. A. Peterson, “Understanding strain and ligand effects in hydrogen evolution over Pd (111) surfaces,” *J. Phys. Chem. C* **118**, 4275–4281 (2014).
- <sup>24</sup>J. R. Kitchin, J. K. Nørskov, M. A. Barteau, and J. G. Chen, “Role of strain and ligand effects in the modification of the electronic and chemical properties of bimetallic surfaces,” *Phys. Rev. Lett.* **93**, 156801 (2004).
- <sup>25</sup>G. Kresse and J. Furthmüller, “Efficiency of ab-initio total energy calculations for metals and semiconductors using a plane-wave basis set,” *Comp. Mater. Sci.* **6**, 15–50 (1996).
- <sup>26</sup>G. Kresse and J. Furthmüller, “Efficient iterative schemes for ab initio total-energy calculations using a plane-wave basis set,” *Phys. Rev. B* **54**, 11169–11186 (1996).
- <sup>27</sup>J. P. Perdew, K. Burke, and M. Ernzerhof, “Generalized gradient approximation made simple,” *Phys. Rev. Lett.* **77**, 3865–3868 (1996).
- <sup>28</sup>J. P. Perdew, K. Burke, and M. Ernzerhof, “Generalized gradient approximation made simple [phys. rev. lett. 77, 3865 (1996)],” *Phys. Rev. Lett.* **78**, 1396–1396 (1997).
- <sup>29</sup>P. E. Blöchl, “Projector augmented-wave method,” *Phys. Rev. B* **50**, 17953–17979 (1994).

- <sup>30</sup>G. Kresse and D. Joubert, “From ultrasoft pseudopotentials to the projector augmented-wave method,” *Phys. Rev. B* **59**, 1758–1775 (1999).
- <sup>31</sup>H. J. Monkhorst and J. D. Pack, “Special points for Brillouin-zone integrations,” *Phys. Rev. B* **13**, 5188–5192 (1976).
- <sup>32</sup>L. Wang, T. Maxisch, and G. Ceder, “Oxidation Energies of Transition Metal Oxides Within the GGA + U Framework,” *Phys. Rev. B* **73**, 195107 (2006).
- <sup>33</sup>C. Franchini, R. Podloucky, J. Paier, M. Marsman, and G. Kresse, “Ground-State Properties of Multivalent Manganese Oxides: Density Functional and Hybrid Density Functional Calculations,” *Phys. Rev. B* **75**, 195128 (2007).
- <sup>34</sup>M. T. Curnan and J. R. Kitchin, “Effects of concentration, crystal structure, magnetism, and electronic structure method on first-principles oxygen vacancy formation energy trends in perovskites,” *J. Phys. Chem. C* **118**, 28776–28790 (2014).
- <sup>35</sup>Z. Xu, J. Rossmeisl, and J. R. Kitchin, “A linear response, dft+u study of trends in the oxygen evolution activity of transition metal rutile dioxides,” *J. Phys. Chem. C In Press* (2015), 10.1021/jp511426q.
- <sup>36</sup>M. García-Mota, A. Vojvodic, F. Abild-Pedersen, and J. K. Nørskov, “Electronic origin of the surface reactivity of transition-metal-doped TiO<sub>2</sub>(110),” *J. Phys. Chem. C* **117**, 460–465 (2013).
- <sup>37</sup>B. Li and H. Metiu, “DFT studies of oxygen vacancies on undoped and doped La<sub>2</sub>O<sub>3</sub> surfaces,” *J. Phys. Chem. C* **114**, 12234–12244 (2010).
- <sup>38</sup>M. García-Mota, A. Vojvodic, H. Metiu, I. C. Man, H.-Y. Su, J. Rossmeisl, and J. K. Nørskov, “Tailoring the activity for oxygen evolution electrocatalysis on rutile TiO<sub>2</sub> (110) by transition-metal substitution,” *ChemCatChem* **3**, 1607–1611 (2011).
- <sup>39</sup>Z. Hu and H. Metiu, “Effect of dopants on the energy of oxygen-vacancy formation at the surface of ceria: Local or global?” *J. Phys. Chem. C* **115**, 17898–17909 (2011).
- <sup>40</sup>Z. Xu and J. R. Kitchin, “Relating the electronic structure and reactivity of the 3d transition metal monoxide surfaces,” *Catal. Commun.* **52**, 60–64 (2014).
- <sup>41</sup>E. W. McFarland and H. Metiu, “Catalysis by doped oxides,” *Chem. Rev.* **113**, 4391–4427 (2013).
- <sup>42</sup>H. Metiu, S. Chrétien, Z. Hu, B. Li, and X. Sun, “Chemistry of Lewis acid–base pairs on oxide surfaces,” *J. Phys. Chem. C* **116**, 10439–10450 (2012).
- <sup>43</sup>J. K. Nørskov, T. Bligaard, J. Rossmeisl, and C. H. Christensen, “Towards the computa-

- tional design of solid catalysts,” *Nat. Chem.* **1**, 37–46 (2009).
- <sup>44</sup>S. Stolbov and S. Zuluaga, “Factors controlling the reactivity of catalytically active monolayers on metal substrates,” *J. Chem. Phys. Lett.* **4**, 1537–1540 (2013).
- <sup>45</sup>J. S. Griffith and L. E. Orgel, “Ligand-field theory,” *Q. Rev. Chem. Soc.* **11**, 381–393 (1957).
- <sup>46</sup>S. A. Akhade and J. R. Kitchin, “Effects of strain, d-band filling, and oxidation state on the surface electronic structure and reactivity of 3d perovskite surfaces,” *J. Chem. Phys.* **137**, 084703 (2012).
- <sup>47</sup>Y.-L. Lee, J. Kleis, J. Rossmeisl, Y. Shao-Horn, and D. Morgan, “Prediction of solid oxide fuel cell cathode activity with first-principles descriptors,” *Energ. Environ. Sci.* **4**, 3966–3970 (2011).
- <sup>48</sup>J. Suntivich, K. J. May, H. A. Gasteiger, J. B. Goodenough, and Y. Shao-Horn, “A perovskite oxide optimized for oxygen evolution catalysis from molecular orbital principles,” *Science* **334**, 1383–1385 (2011).
- <sup>49</sup>A. Vojvodic and J. K. Nørskov, “Optimizing perovskites for the water-splitting reaction,” *Science* **334**, 1355–1356 (2011).
- <sup>50</sup>A. Vojvodic, A. Hellman, C. Ruberto, and B. I. Lundqvist, “From electronic structure to catalytic activity: A single descriptor for adsorption and reactivity on transition-metal carbides,” *Phys. Rev. Lett.* **103**, 146103 (2009).
- <sup>51</sup>See Supplementary Material Document No. for complete details. For information on Supplementary Material, see <http://www.aip.org/pubservs/epaps.html>.
- <sup>52</sup>E. Nikolla, J. Schwank, and S. Linic, “Measuring and relating the electronic structures of nonmodel supported catalytic materials to their performance,” *J. Am. Chem. Soc.* **131**, 2747–2754 (2009).
- <sup>53</sup>S. A. Akhade and J. R. Kitchin, “Effects of strain, d-band filling, and oxidation state on the bulk electronic structure of cubic 3d perovskites,” *J. Chem. Phys.* **135**, 104702 (2011).
- <sup>54</sup>W. A. Harrison, *Electronic Structure and the Properties of Solids: The Physics of the Chemical Bond* (Courier Dover Publications, 2012).
- <sup>55</sup>S. Schnur and A. Groß, “Strain and coordination effects in the adsorption properties of early transition metals: A density-functional theory study,” *Physical Review B* **81**, 033402 (2010).
- <sup>56</sup>A. Vojvodic, J. Nørskov, and F. Abild-Pedersen, “Electronic structure effects in transition

metal surface chemistry,” [Topics in Catalysis](#) **57**, 25–32 (2014).

<sup>57</sup>H. Xin, A. Vojvodic, J. Voss, J. K. Nørskov, and F. Abild-Pedersen, “Effects of *d*-band shape on the surface reactivity of transition-metal alloys,” [Phys. Rev. B](#) **89**, 115114 (2014).